IOPscience iopscience.iop.org

Home Search Collections Journals About Contact us My IOPscience

Global dynamics in the singular logarithmic potential

This article has been downloaded from IOPscience. Please scroll down to see the full text article.

2003 J. Phys. A: Math. Gen. 36 7693

(http://iopscience.iop.org/0305-4470/36/28/302)

View the table of contents for this issue, or go to the journal homepage for more

Download details:
IP Address: 171.66.16.86
The article was downloaded on 02/06/2010 at 16:22

Please note that terms and conditions apply.

INSTITUTE OF PHYSICS PUBLISHING JOURNAL OF PHYSICS A: MATHEMATICAL AND GENERAL

J. Phys. A: Math. Gen. **36** (2003) 7693–7714 PII: S0305-4470(03)58746-7

Global dynamics in the singular logarithmic potential

Cristina Stoica[1] **and Andreea Font**[2]

[1] Department of Mathematics and Statistics, School of ECM, University of Surrey, Guilford, Surrey, GU2 7XH, UK
[2] Department of Physics and Astronomy, University of Victoria, Victoria, BC, V8P 1A1, Canada

E-mail: C.Stoica@surrey.ac.uk and afont@beluga.phys.uvic.ca

Received 23 January 2003, in final form 23 May 2003
Published 1 July 2003
Online at stacks.iop.org/JPhysA/36/7693

Abstract

We present an analytical description of the motion in the singular logarithmic potential of the form $\Phi = \ln \sqrt{x_1^2/b^2 + x_2^2}$, a potential which plays an important role in the modelling of triaxial systems (such as elliptical galaxies) or bars in the centres of galaxy discs. In order to obtain information about the motion near the singularity, we resort to McGehee-type transformations and regularize the vector field. In the axis-symmetric case ($b = 1$), we offer a complete description of the global dynamics. In the non-axis-symmetric case ($b < 1$), we prove that all orbits, with the exception of a negligible set, are centrophobic and retrieve numerically partial aspects of the orbital structure.

PACS numbers: 45.50.Pk, 98.10.+z

1. Introduction

The non-axis-symmetric logarithmic potential plays an important role in galaxy dynamics. In the three-dimensional space, the potential

$$\Phi = \frac{1}{2} \ln \left({R_c}^2 + \frac{{x_1}^2}{b^2} + {x_2}^2 \right) \tag{1.1}$$

(where (x_1, x_2) are the usual cylindrical coordinates $x_1 = z, x_2 = R$) models an elliptical galaxy with a dense core of radius R_c and with the additional property of having a flat rotation curve at large radii [2]. In the 2D space, the logarithmic potential can describe other non-axis-symmetric components of galaxies, such as bars in the centres of galaxy discs.

The study of the orbital structure of the logarithmic potential was initially motivated by the need to construct self-consistent models of galaxies [14]. Numerical experiments have proved to be very useful in revealing the rich orbital structure of this potential, including the major orbit families, the resonances and the stochastic orbits. For example, in the axis-symmetric case ($b = 1$), the logarithmic potential has been shown to admit only loop orbits, which are regular and avoid the origin. The non-axis-symmetric ($b < 1$) potential admits two major

 © 2003 IOP Publishing Ltd Printed in the UK

families of orbits: box (for $\rho = \sqrt{R^2 + z^2} \ll R_c$) and loop orbits (for $\rho \gg R_c$) [1, 11]. Note that this behaviour can also be retrieved from the two simple analytical approximations of the potential, one as a sum of two oscillators very close to the origin and the other one as $\sim\ln(\rho)$ at large distances [2].

An interesting change in the orbital behaviour has been discovered when the potential becomes singular. In their numerical study, Miralda-Escudé and Schwarzschild [10] have found that as $R_c \to 0$, a larger fraction of regular box orbits becomes irregular or 'box-like' (i.e. they will admit fewer integrals of motion than the number of spatial dimensions), with the end result that, in the limit $R_c = 0$, all box orbits are irregular. The general interpretation of this result is that the scattering by the singularity renders the box orbits unstable, a similar behaviour to that observed in systems which contain a central black hole [6]. In addition, the singular logarithmic potential admits several families of minor orbits, i.e., resonances in terms of the x_2:x_1 frequency ratio: the banana (2:1), fish (3:2) and pretzel (4:3) orbits [10]. Numerical studies have also revealed the existence of some stochastic orbits in a narrow region near the singularity [10, 15]. This has led some to suggest a link between the scattering by the singularity and the transition to chaos [3], although no rigorous proof has been given to date in support of this hypothesis.

The present investigation is an analytical approach to the study of the orbital dynamics (including the behaviour near the singularity) in the case of the singular logarithmic potential:

$$\Phi = \frac{1}{2}\ln\left(\frac{{x_1}^2}{b^2} + {x_2}^2\right) \tag{1.2}$$

in both the axis-symmetric and non-axis-symmetric cases. The aim of our work is not only to complement the previous numerical studies performed on this subject, but also to offer a theoretical basis for interpreting their results.

The main difficulty in investigating the system analytically is due to the presence of the singularity in the origin, which creates a discontinuity in the equations of motion. This problem motivates the introduction of a change of coordinates that regularizes the equations of motion. For this, we resort to McGehee-type transformations [9], a technique that is frequently used in celestial mechanics for the study of singularities in the n-body problem ($n = 1, 2, 3, \ldots$). The underlying idea behind this technique is to transform the equations of motions and the time, such that the singularity is 'blown-up' into a non-trivial manifold (in our case a torus). By studying the characteristics of the flow on this manifold, one can extrapolate the information (by continuity with respect to the initial data) about the orbital dynamics around the singularity [13].

The paper is organized as follows. Sections 2 and 3 provide a brief description of our system, in terms of the equations of motion and the conservation of energy. In section 4, we remove the singularity by regularizing the equations of motion. In section 5, we provide a description of the collision manifold and the zero-velocity manifold, two abstract surfaces on which we can visualize the properties of the flow close to the singularity and at the maximum distance from the source allowed for a given energy, respectively. Section 6 presents the complete global dynamics in the axis-symmetric case ($b = 1$). In section 7, we extend the analysis for the case of the non-axis-symmetric potential ($b \neq 1$), in the restricted limit in which the anisotropy is small. In this case, we prove theoretically that the majority of orbits in this case are centrophobic (that is, they avoid the origin)—a result that has been originally discovered in the numerical study of Miralda-Escudé and Schwarzschild [10]—and we discuss the orbital structure in terms of orbits which preserve or change the sign of their angular momentum. Finally, in section 8, we show how several families of resonances can be retrieved through the numerical integration of the new system of equations.

2. The equations of motion

The non-axis-symmetric logarithmic problem is a one-parameter Hamiltonian system with two degrees of freedom. The anisotropic logarithmic singular potential (1.2) determines a conservative system with a preserved Hamiltonian given by

$$H(x_1, x_2, y_1, y_2) = \frac{1}{2}\left({y_1}^2 + {y_2}^2\right) + \ln\left(\sqrt{\frac{{x_1}^2}{b^2} + {x_2}^2}\right) \tag{2.1}$$

where $(x_1, x_2) \in \mathbb{R}^2_+ - \{(0,0)\}$ are the generalized coordinates and $(y_1, y_2) \in \mathbb{R}$ are the momenta.

We start by writing the equations of motion in a form that contains the anisotropy in the kinetic term rather than in the potential. Thus, we substitute $q_1 = x_1/b^2$, $q_2 = x_2$, and $p_1 = y_1/b^2$, $p_2 = y_2$. Introducing the (standard) notation for the generalized vector coordinate $\mathbf{q} = (q_1, q_2)$, the generalized momenta $\mathbf{p} = (p_1, p_2)$, the anisotropy parameter $\mu = \frac{1}{b^2}$ and the mass matrix

$$M = \begin{pmatrix} \mu & 0 \\ 0 & 1 \end{pmatrix}$$

the Hamiltonian can be written as

$$H(\mathbf{q}, \mathbf{p}) = \tfrac{1}{2}\mathbf{p}^T M \mathbf{p} + \ln|\mathbf{q}| \tag{2.2}$$

and the anisotropic logarithmic problem is given as the first-order system of ordinary differential equations:

$$\begin{cases} \dot{\mathbf{q}} = M\mathbf{p} \\ \dot{\mathbf{p}} = -\frac{\mathbf{q}}{|\mathbf{q}|^3}. \end{cases} \tag{2.3}$$

When $\mu = 1$, the above system describes the motion in the axis-symmetric logarithmic potential. From the point of view of Hamiltonian mechanics this case is completely integrable, as we have the two integrals of motion given by the conservation of the total energy and the total angular momentum. However, we point out that for $|\mathbf{q}| \to 0$ the dynamical behaviour becomes unknown since the vector field $(\dot{\mathbf{q}}, \dot{\mathbf{p}})$ ceases to exist.

Let K be the kinetic energy,

$$K = \tfrac{1}{2}\mathbf{p}^T M \mathbf{p} \tag{2.4}$$

and V the potential,

$$V = \ln|\mathbf{q}|. \tag{2.5}$$

The total energy E is then

$$H(\mathbf{q}, \mathbf{p}) = K + V. \tag{2.6}$$

Since the system (2.3) is Hamiltonian the total energy is conserved. That is $H(\mathbf{q}, \mathbf{p})$ is constant along the solution curves of (2.3) and consequently the level sets of $H(\mathbf{q}, \mathbf{p})$ are invariant under the flow. If h is a certain energy constant (i.e. $H(\mathbf{q}, \mathbf{p}) = h = \text{constant}$) then the level set $H(\mathbf{q}, \mathbf{p})^{-1}(h)$ is a three-dimensional surface usually called an *energy surface,* which we denote by Σ_h.

3. Topological description of the energy surfaces

We consider in more detail the topology of various surfaces Σ_h, including the orbits near the singularity. Let us fix $h \in \mathbb{R}$. Using a technique similar to McGehee's [9] we introduce the change of variables:

$$\begin{cases} \mathbf{q} = r\,\mathrm{e}^{-\frac{1}{r^2}}\mathbf{s} \\ \mathbf{p} = \frac{1}{r}\mathbf{u} \end{cases} \tag{3.1}$$

where $r > 0, \mathbf{s}$ is a point on the unit circle $\mathbb{S}^1$ and $\mathbf{u} \in \mathbb{R}^2$. Our transformation is a diffeomorphism from $\mathbb{R}^2 \setminus \{(0,0)\} \times \mathbb{R}^2$ to $(0,\infty) \times \mathbb{S}^1 \times \mathbb{R}^2$ (where $\mathbb{S}^1$ is the unit circle) and can be understood as a passing to some unorthodox kind of polar coordinates.

The system (2.3) becomes

$$\begin{cases} \dot{r} = \dfrac{r}{r^2+2}\,\mathrm{e}^{\frac{1}{r^2}}\mathbf{s}^T M\mathbf{u} \\ \dot{\mathbf{s}} = \dfrac{1}{r^2}\,\mathrm{e}^{\frac{1}{r^2}}[M\mathbf{u} - (\mathbf{s}^T M\mathbf{u})\cdot\mathbf{s}] \\ \dot{\mathbf{u}} = \mathrm{e}^{\frac{1}{r^2}}\left[\dfrac{1}{r+2}(\mathbf{s}^T M\mathbf{u})\cdot\mathbf{u} - \mathbf{s}\right] \end{cases} \tag{3.2}$$

and the conservation of energy transforms to

$$\tfrac{1}{2}\mathbf{u}^T M\mathbf{u} + r^2\ln r - 1 = hr^2. \tag{3.3}$$

Note that the new system (3.2) is analytic on the open manifold $(0,\infty) \times \mathbb{S}^1 \times \mathbb{R}^2$ and that the regions of motion are constrained by the energy relation (3.3). More precisely, since the kinetic term in (3.3) is positive, we have that for a fixed level of energy h:

$$hr^2 - r^2\ln r + 1 \geqslant 0. \tag{3.4}$$

Solving the above relation, it follows that $0 < r < R_{\max}$ with $R_{\max} = R_{\max}(h)$. In other words the motion is always bounded for any fixed level of energy h. Also, we can say that the energy surface Σ_h projects onto a disc of radius $R_{\max}$ in $\mathbb{R}^2 \setminus (0,0)$. Since

$$\tfrac{1}{2}\mathbf{u}^T M\mathbf{u} = hr^2 - r^2\ln r + 1 \tag{3.5}$$

it follows that along the $r = R_{\max}$ boundary we have $\mathbf{u} = \mathbf{0}$, that is the kinetic term cancels. For this reason the curve

$$\begin{cases} r = R_{\max} \\ \mathbf{u} = \mathbf{0} \end{cases} \tag{3.6}$$

is called the *oval of zero velocity* in Σ_h. In physical space, this curve represents the outermost boundary of the orbital structure allowed for a given energy. We will denote this curve by Z.

Proposition 3.1. *For any fixed level of energy h the energy surface Σ_h is diffeomorphic to an open solid torus (i.e., a solid torus minus its boundary).*

Proof. The proof follows closely the proof of proposition 1.1 in [4]. Let B be the interior of the ellipse

$$\tfrac{1}{2}\mathbf{u}^T M\mathbf{u} = 1$$

in the plane. Clearly B is topologically equivalent to $\mathbb{S}^1 \times (0, R_{\max}]$ ($r = 0$ corresponds to the missing boundary of the ellipse). Then we define $F : \Sigma_h \longrightarrow \mathbb{S}^1 \times B$ by

$$F(r, \mathbf{s}, \mathbf{u}) = (\mathbf{s}, \mathbf{u}).$$

F is just the required diffeomorphism. □

4. Regularization of the vector field

The objective of this section is twofold: to extend the energy relation to $r = 0$, and to regularize the system (3.3) such that the new vector field becomes differentiable over the entire interval $r \in [0, R_{\max}]$.

The energy relation (3.3) is ill-defined at the singularity $r = 0$. However, the function $r^2 \ln r$ can be continuously extended for $r = 0$ by

$$f(r) = \begin{cases} r^2 \ln r & \text{if} \quad r > 0 \\ 0 & \text{if} \quad r = 0. \end{cases} \tag{4.1}$$

The extended function (4.1) is also differentiable over its domain. Therefore we are able to extend the energy manifold by

$$\tfrac{1}{2}\mathbf{u}^T M\mathbf{u} + f(r) - 1 = hr^2 \tag{4.2}$$

for all $r \in [0, R_{\max}]$.

Now we will introduce a sequence of transformations of the system (3.2) such that the new system will have no singularity at $r = 0$. Following the technique introduced by McGehee [9], we want to paste an invariant manifold onto the phase space, such that we close the open solid torus that bounds the motion, by including its boundary $r = 0$. Also, in order to preserve the continuity of the flow with respect to the initial data, we have to ensure that the transformed system has a differentiable vector field.

We implement a change of the time variable through $\mathrm{d}\sigma = -\mathrm{e}^{\frac{1}{r^2}} r^2\, \mathrm{d}t$. This will have the effect of decreasing the rate of the time intervals near the singularity. Expressed in the new time derivative $\frac{\mathrm{d}}{\mathrm{d}\sigma}$, the system (3.2) becomes

$$\begin{cases} \dot{r} = -\frac{r^3}{r^2+2}\mathbf{s}^T M\mathbf{u} \\ \dot{\mathbf{s}} = (\mathbf{s}^T M\mathbf{u})\cdot\mathbf{s} - M\mathbf{u} \\ \dot{\mathbf{u}} = r^2\left[\mathbf{s} - \frac{1}{r^2+2}(\mathbf{s}^T M\mathbf{u})\cdot\mathbf{u}\right]. \end{cases} \tag{4.3}$$

We note that by the above sequence of reparametrizations we have obtained an analytic vector field for $(r, \mathbf{s}, \mathbf{u}) \in [0, R_{\max}] \times \mathbb{S}^1 \times \mathbb{R}^2$, which is coupled with a differentiable integral relation given by (4.2).

It follows from (4.2) that each energy surface Σ_h meets the boundary $r = 0$ along a submanifold given by

$$\begin{cases} \frac{1}{2}\mathbf{u}^T M\mathbf{u} = 1 \\ \mathbf{s} \ \text{ arbitrary.} \end{cases} \tag{4.4}$$

This manifold, let us call it Λ, is diffeomorphic with a two-dimensional torus, which we shall call the *collision manifold*. This fictitious torus has no meaning in the physical space, since the motion ceases to exist in the origin. However, the behaviour of the orbits near the singularity can be extrapolated from similar properties of the flow on the collision manifold. In this sense, we regard the differential system of equations as a vector field on the manifold, its solutions representing the flow.

Note that Λ is independent of the total energy and therefore we can say that the time transformations we have applied have the effect of pasting an invariant boundary onto each Σ_h. Over this boundary the vector field is given by

$$\begin{cases} \dot{\mathbf{s}} = (\mathbf{s}^T M\mathbf{u})\cdot\mathbf{s} - M\mathbf{u} \\ \dot{\mathbf{u}} = \mathbf{0}. \end{cases} \tag{4.5}$$

The solid and now compact torus Σ_h bounds all the orbits and by investigating its properties, one can obtain a global picture of the motion, including the motion near the singularity. We emphasize that the orbits of system (2.3) are the same as the orbits of system (4.3), only the parametrization is different. Therefore, any results concerning the solutions of the first system can be seen as results for the solutions of the second, as long as one is aware of the fact that the rate at which solutions move along the orbits is different.

Using the energy integral we can further reduce the dimension of the system. For this, we express the coordinates $(\mathbf{s}, \mathbf{u})$ in terms of the new angle coordinates θ and ψ:

$$\begin{cases} \mathbf{s} = (\cos\theta, \sin\theta) \\ \mathbf{u} = \sqrt{2(hr^2 - f(r) + 1)}\left(\dfrac{1}{\sqrt{\mu}}\cos\psi, \sin\psi\right). \end{cases} \tag{4.6}$$

Also, in order to further simplify the system, we perform a similar time parametrization which incorporates a part of the radial dependence in a new time variable:

$$\mathrm{d}s = \sqrt{2(hr^2 - f(r) + 1)}\,\mathrm{d}\sigma. \tag{4.7}$$

In these variables, the system (4.3) becomes a first-order system for $(r, \theta, \psi) \in [0, R_{\max}] \times \mathbb{S}^1 \times \mathbb{S}^1$ with a differentiable vector field:

$$\begin{cases} \dot{r} = -\left(\dfrac{r^3}{r^2+2}\right) 2(hr^2 - f(r) + 1)(\sqrt{\mu}\cos\theta\cos\psi + \sin\theta\sin\psi) \\ \dot{\theta} = 2(hr^2 - f(r) + 1)(\sqrt{\mu}\cos\psi\sin\theta - \sin\psi\cos\theta) \\ \dot{\psi} = r^2(\cos\psi\sin\theta - \sqrt{\mu}\sin\psi\cos\theta). \end{cases} \tag{4.8}$$

Before discussing different aspects of the dynamics of the above system, we make two more observations.

Observation 1. Up to this point, no reference was made to the angular momentum integral. It is well known that in the axis-symmetric case ($\mu = 1$), the singular logarithmic system admits, besides the total energy, a second conserved quantity, namely the angular momentum $C := q_2 p_1 - q_1 p_2$. In terms of (r, θ, ψ) this reads

$$C(s) = \mathrm{e}^{-1/r^2} 2[hr^2 - f(r) + 1][\sqrt{\mu}\sin\theta\cos\psi - \cos\theta\sin\psi] \tag{4.9}$$

where s is the final time variable introduced in (4.7).

Like the energy relation, $C(s)$ is ill-defined at the singularity. In an analogous way, we extend the function e^{-1/r^2} continuously at $r = 0$ by defining the function

$$g(r) = \begin{cases} \mathrm{e}^{-1/r^2} & \text{if} \quad r > 0 \\ 0 & \text{if} \quad r = 0. \end{cases} \tag{4.10}$$

The angular momentum is now well defined and differentiable for all $r \geqslant 0$. For the axis-symmetric case ($\mu = 1$), the law of conservation of angular momentum ensures that

$$\frac{\mathrm{d}C}{\mathrm{d}s} = 0 \tag{4.11}$$

and therefore we have the integral relation

$$C(s) = g(r)2[hr^2 - f(r) + 1]\sin(\theta - \psi) = \text{ const.} \tag{4.12}$$

In the anisotropic case ($\mu \neq 1$) the above symmetry is lost. The anisotropy is responsible for the much more complicated dynamics and, eventually, for the existence of the chaotic motion. For later purposes, we write the variation of angular momentum

$$\frac{\mathrm{d}C}{\mathrm{d}t} = (1 - \mu)p_1 p_2 \tag{4.13}$$

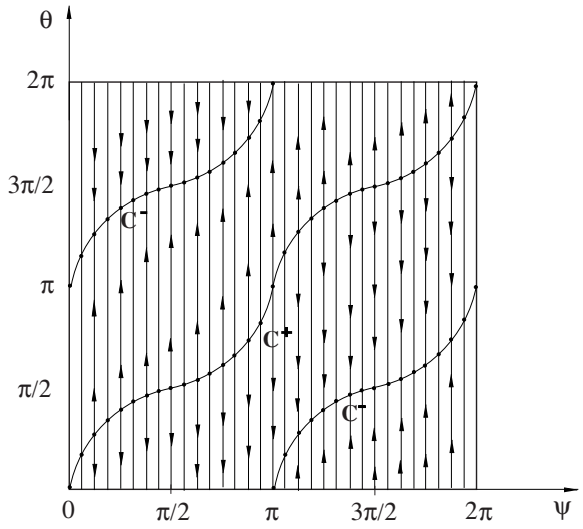

Figure 1. On the collision manifold, the flow follows the parallel lines $\psi = \psi_0 = \text{const}$. The flow vanishes on the equilibrium curves C^+ and C^-.

in terms of the new variables and time:

$$\frac{\mathrm{d}}{\mathrm{d}s}(\mathrm{e}^{-1/r^2}\dot{\theta}) = \frac{1-\mu}{\sqrt{\mu}}\,\mathrm{e}^{-1/r^2}2[hr^2 - f(r) + 1]^{3/2}\sin\psi\cos\psi. \tag{4.14}$$

Observation 2. The orbital dynamics of the system (4.8) does not depend on the level of energy h. More precisely, each different but fixed h gives rise to the same qualitative phase portrait. The only change is in the value of $R_{\max}$, as $R_{\max}$ depends directly on h. Therefore, without losing generality, and in order to simplify the calculations, we choose from now on to work with $h = 0$.

5. The collision manifold and the zero-velocity manifold

The flow on the invariant collision manifold Λ is given by imposing the restriction $r = 0$ to the system (4.8):

$$\begin{cases} \dot{\theta} = 2(\sqrt{\mu}\cos\psi\sin\theta - \sin\psi\cos\theta) \\ \dot{\psi} = 0. \end{cases} \tag{5.1}$$

We obtain a family of solutions $\psi = \psi_0 = \text{const}$, whereas the vector field vanishes along the deformed circles $\{(\theta, \psi)|\psi = \psi_0, \sqrt{\mu}\cos\psi_0\sin\theta - \sin\psi_0\cos\theta = 0\}$. Note that for $\mu = 1$, the curves of equilibria transform into circles given by $\{(\theta, \psi)|\psi = \psi_0, \theta = \psi_0, \theta = \pi + \psi_0\}$. For the general case $\mu \neq 1$, let us denote by C^+ the equilibrium curve that passes through $\theta = \psi = 0$ and by C^- the curve that passes through $\theta = \psi = \pi$. It is immediate that C^+ is a repeller and C^- is an attractor. The dynamical behaviour on the collision manifold Λ is illustrated in figure 1. Since $\dot{\psi} = 0$, the flow follows the parallel lines $\psi = \psi_0 = \text{const}$.

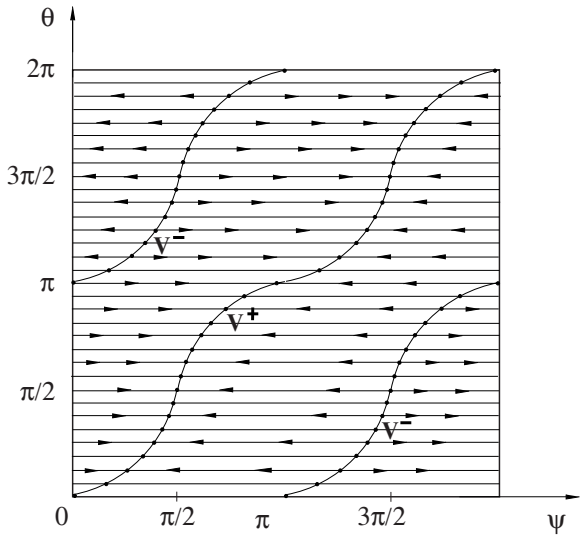

Figure 2. On the zero-velocity manifold, the flow follows the parallel lines $\theta = \theta_0 = \text{const}$. The flow vanishes on the equilibrium curves V^+ and V^-.

Similarly, for $r = R_{\max}$ we obtain another invariant manifold $\Omega = \Omega_h$ for (4.8), namely the manifold corresponding to the oval of zero velocity. Recall that $R_{\max}$ is the value which cancels $hr^2 + 1 - f(r) = 1 - f(r)$ (h is set to zero). The flow on Ω is given by

$$\begin{cases} \dot{\theta} = 0 \\ \dot{\psi} = R_{\max}^2(\cos\psi \sin\theta - \sqrt{\mu}\sin\psi\cos\theta). \end{cases} \tag{5.2}$$

The dynamical behaviour on the zero-velocity manifold is similar to that on the collision manifold: the torus $(r, \theta, \psi) \in R_{\max} \times \mathbb{S}^1 \times \mathbb{S}^1$ that represents Ω_0 is covered by orbits parallel to $\theta = \theta_0 = \text{const}$. There are again, two skewed circles of equilibria, $\{(\theta, \psi)|\theta = \theta_0, \cos\psi\sin\theta - \sqrt{\mu}\sin\psi\cos\theta = 0\}$. Denoting by V^+ the curve that passes through $(0, 0)$ and by V^- the curve that passes through $(0, \pi)$, it follows that V^+ is an attractor and V^- is a repeller (see figure 2).

6. Global dynamics of the axis-symmetric system ($\mu = 1$)

We now return to the full system (4.8) and, taking into account that (at least in a prime analysis) the anisotropy is given by values of μ close to 1 but greater than 1, we define the parameter $\epsilon := \sqrt{\mu} - 1 > 0$, which we will later treat as a small perturbation to the isotropic system. We also choose to work with the relative angle $\varphi := \theta - \psi$, instead of the angle θ. Then, written in terms of ϵ and (r, φ, ψ) and neglecting the terms of order ϵ^2 and higher, the system (4.8) becomes

$$\begin{cases} \dot{r} = -\dfrac{r^3}{r^2+2}2(1 - f(r))[\cos\varphi + \epsilon\cos(\varphi+\psi)\cos\psi] \\ \dot{\varphi} = [2(1 - f(r)) - r^2]\sin\varphi \\ \qquad\quad + \epsilon[2(1 - f(r))\cos\psi\sin(\varphi+\psi) + r^2\sin\psi\cos(\varphi+\psi)] \\ \dot{\psi} = r^2[\sin\varphi - \epsilon\sin\psi\cos(\varphi+\psi)]. \end{cases} \tag{6.1}$$

In the absence of the small perturbation ($\epsilon = 0$), that is in the axis-symmetric case $\mu = 1$, the above system reduces to

$$\begin{cases} \dot{r} = -\dfrac{r^3}{r^2+2} 2(1 - f(r)) \cos\varphi \\ \dot{\varphi} = [2(1 - f(r)) - r^2] \sin\varphi \\ \dot{\psi} = r^2 \sin\varphi \end{cases} \tag{6.2}$$

with (r, φ, ψ) on the solid torus $[0, R_{\max}] \times \mathbb{S}^1 \times \mathbb{S}^1$. The equilibrium solutions form two circles along $\varphi = 0$ and $\varphi = \pi$ and are given by $(0, 0, \psi_0)$ and $(0, \pi, \psi_0)$ where ψ_0 can be any value in $[0, 2\pi]$.

There are four invariant manifolds:

- the collision manifold (at $r = 0$), on which the dynamics is given by

$$\begin{cases} \dot{\varphi} = 2 \sin\varphi \\ \dot{\psi} = 0. \end{cases} \tag{6.3}$$

- the zero-velocity manifold (at $r = R_{\max}$), on which we have

$$\begin{cases} \dot{\varphi} = -R_{\max}^2 \sin\varphi \\ \dot{\psi} = R_{\max}^2 \sin\varphi \end{cases} \tag{6.4}$$

  or just $\frac{\mathrm{d}\varphi}{\mathrm{d}\psi} = -1$.
- the '$\sin\varphi = 0$' manifolds (when $\varphi = 0$ or $\varphi = \pi$), with

$$\begin{cases} \dot{r} = -\dfrac{r^3}{r^2+2} 2(1 - f(r)) & \text{if} \quad \varphi = 0 \\ \dot{r} = \dfrac{r^3}{r^2+2} 2(1 - f(r)) & \text{if} \quad \varphi = \pi. \end{cases} \tag{6.5}$$

Recall that in the unperturbed case the angular momentum is conserved. In this case (see observation 1):

$$C(s) = g(r) 2(1 - f(r)) \sin\varphi = C = \text{ const} \tag{6.6}$$

for all $r \in [0, R_{\max}]$. It is easy to see that

$$C = 0 \quad \Longleftrightarrow \quad [r = 0 \,\text{or}\, r = R_{\max} \,\text{or}\, \sin\varphi = 0]. \tag{6.7}$$

In other words, the angular momentum is null (i.e. the motion is rectilinear) if and only if the orbits are either on the collision manifold, or on the zero-velocity manifold, or connecting the two. From this perspective, we can denote the surfaces '$\sin\varphi = 0$' as manifolds of zero angular momentum. Thus we have:

Proposition 6.1. *In the axis-symmetric singular logarithmic problem the only orbits reaching the collision are the rectilinear ones.*

Proposition 6.2. *In the axis-symmetric singular logarithmic problem all orbits with nonzero angular momentum are bounded, they do not fall/eject into/from the source, and they do not reach maximum distance with respect to the source.*

We return to the analysis of the unperturbed system (6.2) and note that the system decouples in the sense that the first two equations are independent of ψ. Thus, if one solves the equations of r and φ, then ψ is obtained by replacing the expressions for r and φ into the third equation

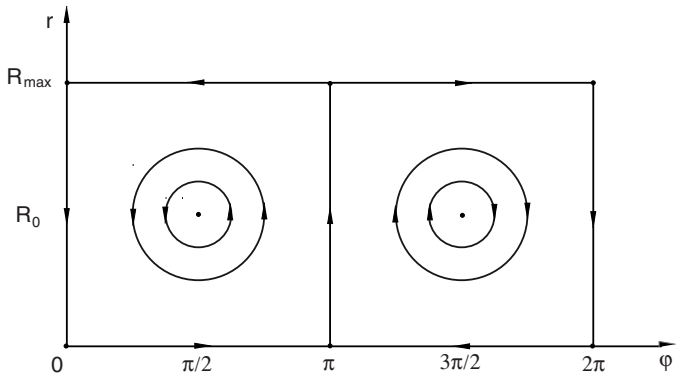

Figure 3. The reduced phase space (r, φ) in the case $\mu = 1$. There are six equilibrium points: two centres, $(R_0, \pi/2)$ and $(R_0, 3\pi/2)$, and four saddle equilibria, $(0, 0)$, $(0, \pi)$, $(R_{\max}, 0)$ and $(R_{\max}, \pi)$.

and then integrating. Therefore, a detailed qualitative analysis of the reduced system

$$\begin{cases} \dot{r} = -\dfrac{r^3}{r^2+2} 2(1 - f(r)) \cos\varphi \\ \dot{\varphi} = [2(1 - f(r)) - r^2] \sin\varphi \end{cases} \tag{6.8}$$

is extremely useful, as it may be extended to the full (r, φ, ψ) space by introducing the third coordinate ψ at the end of our investigation.

The reduced system is relatively easy to describe. The motion takes place on the cylinder $[0, R_{\max}] \times \mathbb{S}^1$. There are four degenerate saddle equilibria located at $(0, 0)$, $(0, \pi)$, $(R_{\max}, 0)$, $(R_{\max}, \pi)$, and two centres at $(R_0, \pi/2)$ and $(R_0, 3\pi/2)$, where R_0 is the solution of the equation $2(1 - f(r)) - r^2 = 0$. A direct computation shows that the eigenvalues for the centres are given by $\lambda_{1,2} = \pm i R_0^2 \sqrt{2(R_0^2 + 2)/(R_0 + 2)}$. Also, there are four invariant manifolds $\{r = 0\}$, $\{r = R_{\max}\}$, $\{\varphi = 0\}$ and $\{\varphi = \pi\}$, forming two heteroclinic cycles connecting the saddle equilibria (see figure 3).

We now lift the dynamics from the (r, φ) phase space into the full (r, φ, ψ) solid torus by taking into consideration the third $\psi \in \mathbb{S}^1$ coordinate, as well as the dynamics on the collision manifold, zero-velocity manifold and the '$\sin\varphi = 0$' zero angular momentum manifolds.

The global flow, which takes place in the solid torus $[0, R_{\max}] \times \mathbb{S}^1 \times \mathbb{S}^1$, can be seen in figure 4 and is represented as follows:

- The outside boundary corresponds to the collision manifold $\{r = 0\}$.
- The interior boundary corresponds to $\{r = R_{\max}\}$. The centred circle of the torus was 'blown up' artificially to an inside torus such that the dynamics on the zero-velocity manifold can be seen (this is just a visual artefact and does not modify the analysis).
- The motion takes place in between the exterior boundary $\{r = 0\}$ and the interior boundary $\{r = R_{\max}\}$.
- The surface of zero angular momentum '$\sin\varphi = 0$' divides the space into two distinct global invariant manifolds: one corresponding to $\varphi \in (0, \pi)$ or, equivalently, to motion with positive angular momentum ($C > 0$), and the other corresponding to $\varphi \in (\pi, 2\pi)$ or simply, to $C < 0$; the flow is symmetric with respect to the horizontal plane $C = 0$. In this latter plane, the physical motion is rectilinear and represents orbits that are ejecting from the collision manifold, reaching the maximum distance at the zero-velocity manifold and falling back on the collision manifold.

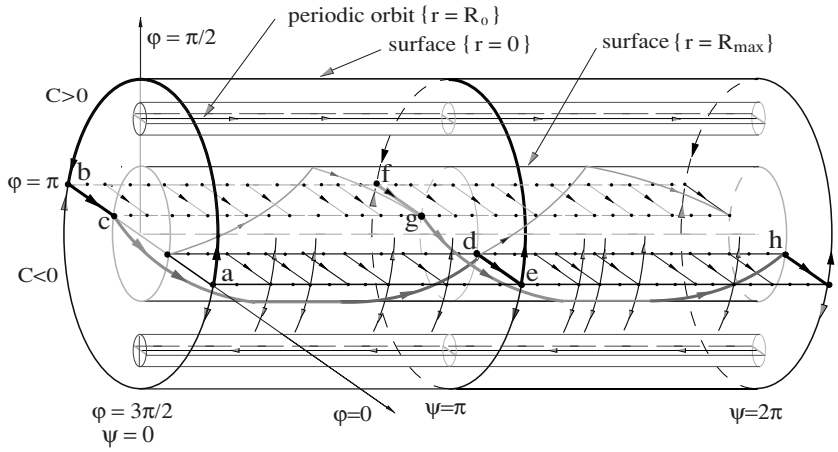

Figure 4. The global flow in the axis-symmetric case ($\mu = 1$), described in a solid torus delineated by the two surfaces $\{r = 0\}$ and $\{r = R_{\max}\}$. The full lines denote the heteroclinic cycle for the case $\psi_0 = 0$. The horizontal plane ($C = 0$) divides the phase space into two symmetric invariant subspaces (see text for details).

- There are two periodic orbits situated symmetrically with respect to the horizontal plane ($C = 0$), namely $\{(r, \varphi, \psi) | r = R_0, \varphi = \pi/2, \psi = \psi_0 + R_0 s; s \geqslant 0, \psi_0 = \psi(0)\}$ and $\{(r, \varphi, \psi) | r = R_0, \varphi = 3\pi/2, \psi = \psi_0 - R_0 s; s \geqslant 0, \psi_0 = \psi(0)\}$. Around those two periodic orbits, the phase space is foliated by tori-like surfaces, parametrized by the angular momentum integral (6.6).
- The equilibria on the collision manifold are connected with the equilibria on the zero-velocity manifold, through heteroclinic cycles of the form

$$a \longrightarrow b \longrightarrow c \longrightarrow d \longrightarrow e \longrightarrow f \longrightarrow g \longrightarrow h \longrightarrow a$$

  where $a = (0, 0, \psi_0)$, $b = (0, \pi, \psi_0)$, $c = (R_{\max}, \pi, \psi_0)$, $d = (R_{\max}, 0, \psi_0 + \pi)$, $e = (0, 0, \psi_0 + \pi)$, $f = (0, \pi, \psi_0 + \pi)$, $g = (R_{\max}, \pi, \psi_0 + \pi)$ and $h = (R_{\max}, 0, \psi_0 + 2\pi) \equiv (R_{\max}, 0, \psi_0)$, for each fixed ψ_0 fixed in $[0, 2\pi]$ corresponding to one cycle.

Let us look at the surfaces with positive values of the angular momentum, $C > 0$ (for negative C, by symmetry, the flow is identical but in the opposite sense). Since each value $C = \text{const}$ represents a tori-like surface, the space contains a series of invariant manifolds nested one into the other. C varies from 0 to a maximal value corresponding to the degenerate torus $r = R_0$, i.e. a circle (see figure 5).

The dynamics will change as one shifts from the tori close to $C = 0$ towards the tori near the periodic orbit $r = R_0$. In the (φ, ψ) plane, the orbits close to the collision manifold $\{r = 0\}$ have very large slopes $\mathrm{d}\varphi/\mathrm{d}\psi$ (for example, the orbits on c_1 in figure 5). The orbits close to the periodic orbit $r = R_0$ have slopes close to -1 (e.g., the orbits on c_3 in figure 5). In between, there is a smooth transition in the values of the slopes (one has to keep in mind that the flow is continuous and therefore orbits which are initially close have to stay close at all times).

For a fixed value of C or, in other words, for a fixed torus, the motion is bounded between a minimum and a maximum value, which depend directly on C. We note that in the real physical space (x_1, x_2), this translates into a bounded motion between a minimum and a maximum value, representing a loop orbit. The periodic solutions, $(R_0, \pi/2, \psi)$ and $(R_0, 3\pi/2, \psi)$,

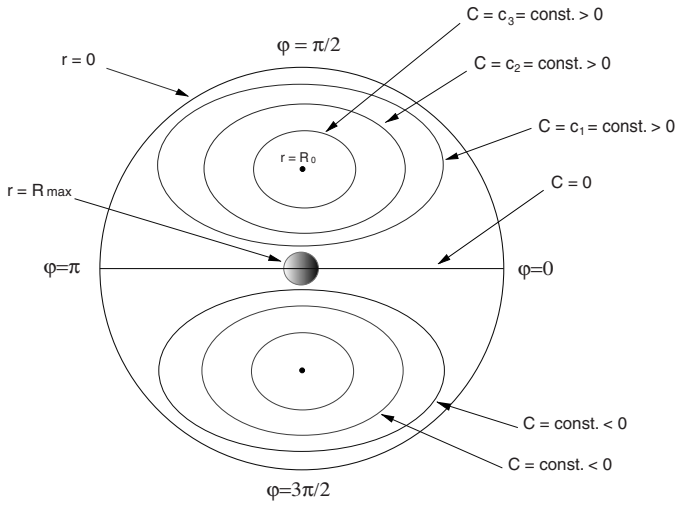

Figure 5. Section on the solid torus at $\psi = \psi_0$. Around the two periodic orbits $r = R_0$, the phase space is foliated by tori-like surfaces of constant angular momentum, C.

correspond to the two parent families of the loop orbits, one anticlockwise ($C > 0$) and the other clockwise ($C < 0$) [2]. We shall discuss the family of loop orbits in more detail in sections 7 and 8.

7. Dynamics of the non-axis-symmetric system ($\mu \neq 1$)

In this section, we proceed to investigate the general form of the non-axis-symmetric system (6.1). We will limit our analysis to the case in which the anisotropy is small ($\mu \simeq 1$) and therefore we can treat it as a small perturbation ($\epsilon = \sqrt{\mu} - 1 > 0$) to the isotropic system.

In the following, we derive the curves of equilibria on the collision manifold and on the zero-velocity manifold. We observe that these curves, located in the horizontal plane ($C = 0$), remain upon the perturbation within $O(\epsilon)$ distance of this plane. We then prove that most orbits in the perturbed case avoid the origin, a result initially discovered in the numerical study of Miralda-Escudé and Schwarzschild [10]. For this, we show that the curves of equilibria on the collision manifold are degenerate saddles, i.e. the equilibrium points on these curves admit a 2D stable and a 2D unstable manifold. The implication is that, in the three-dimensional space, the dimension of the set of initial conditions leading to collision is 2 (i.e., the Lebesgue measure of the set is zero). In physical space this translates into a zero probability of finding orbits falling into the source.

Lemma 7.1. *The equilibria of the vector field (6.1) consist of four closed curves, two belonging to the collision manifold and the other two to the zero-velocity manifold. The collision manifold curves of equilibria are given by*

$$C_1 := \{(r, \varphi, \psi) \mid r = 0, \varphi = \arctan[(1-\epsilon)\tan\psi] - \psi, \psi = \psi_0 \in [0, 2\pi)\} \cup \cup(0, 0, \pi/2) \cup (0, 0, 3\pi/2) \tag{7.1}$$

and

$$C_2 := \{(r, \varphi, \psi) \mid r = 0, \varphi = \pi + \arctan[(1-\epsilon)\tan\psi] - \psi, \psi = \psi_0 \in [0, 2\pi)\} \cup \cup(0, \pi, \pi/2) \cup (0, \pi, 3\pi/2). \tag{7.2}$$

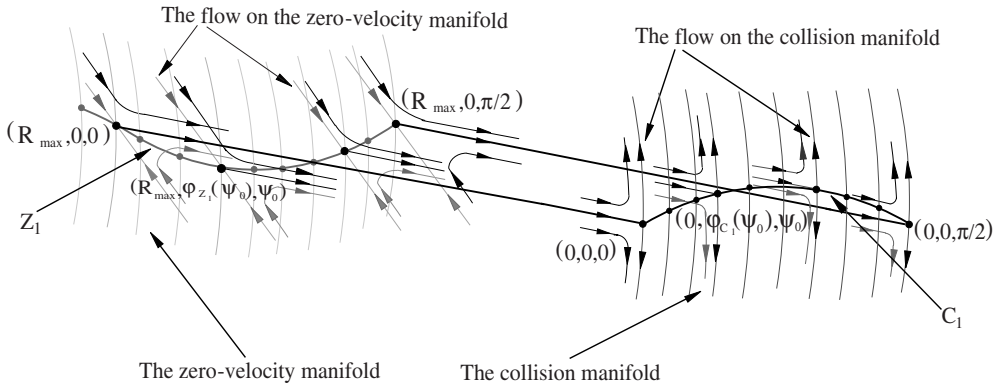

Figure 6. The curves of equilibria Z_1 and C_1, located on the collision manifold and on the zero-velocity manifold, respectively. Each equilibrium point on these two curves behaves like a degenerate saddle.

The curves of equilibria on the zero-velocity manifold are given by

$$Z_1 := \{(r, \varphi, \psi) \mid r = R_{\max}, \varphi = \arctan[(1+\epsilon)\tan\psi] - \psi, \psi = \psi_0 \in [0, 2\pi)\} \cup (R_{\max}, 0, \pi/2) \cup (R_{\max}, 0, 3\pi/2) \tag{7.3}$$

and

$$Z_2 := \{(r, \varphi, \psi) \mid r = R_{\max}, \varphi = \pi + \arctan[(1+\epsilon)\tan\psi] - \psi, \psi = \psi_0 \in [0, 2\pi)\} \cup (R_{\max}, \pi, \pi/2) \cup (R_{\max}, \pi, 3\pi/2). \tag{7.4}$$

Proof. The proof follows by inspection. One can verify directly that the two families of curves cancel the vector field. To see that there are no other equilibria, suppose $r \neq 0$ and $r \neq R_{\max}$. Then $\dot{r} = 0$ and $\dot{\psi} = 0$ lead to

$$\begin{cases} (1+\epsilon)\cos(\varphi+\psi)\cos\psi = -\sin(\varphi+\psi)\sin\psi \\ (1+\epsilon)\cos(\varphi+\psi)\sin\psi = \sin(\varphi+\psi)\cos\psi. \end{cases}$$

It is easy to check that the above relations cannot coexist. □

Observation 7.2. C_1 and C_2 are within $O(\epsilon)$ distance of the circles

$$\{(r, \varphi, \psi) \mid r = 0, \varphi = 0, \psi = \psi_0 \in [0, 2\pi)\}$$

and respectively,

$$\{(r, \varphi, \psi) \mid r = 0, \varphi = \pi, \psi = \psi_0 \in [0, 2\pi)\}.$$

Also, on the zero-velocity manifold, Z_1 and Z_2 are within $O(\epsilon)$ distance of the circles

$$\{(r, \varphi, \psi) \mid r = R_{\max}, \varphi = 0, \psi = \psi_0 \in [0, 2\pi)\}$$

and

$$\{(r, \varphi, \psi) \mid r = R_{\max}, \varphi = \pi, \psi = \psi_0 \in [0, 2\pi)\}$$

respectively.

Lemma 7.3. *The curves of equilibria Z_1 and Z_2 on the zero-velocity manifold are degenerate saddles (see figure 6). More precisely, for a fixed ψ_0, the two corresponding equilibria*

$$(R_{\max}, \arctan[(1+\epsilon)\tan\psi_0] - \psi_0, \psi_0) \in Z_1$$

and

$$(R_{\max}, \pi + \arctan[(1+\epsilon)\tan\psi_0] - \psi_0, \psi_0) \in Z_2$$

behave like saddles in the (r, φ) *plane.*

Proof. Recall from section 6 that on the zero-velocity manifold the flow is degenerate and in the (φ, ψ) coordinates it reads

$$\begin{cases} \dot{\varphi} = -R_{\max}^2[\sin(\varphi+\psi)\cos\psi - (1+\epsilon)\cos(\varphi+\psi)\sin\psi] \\ \dot{\psi} = R_{\max}^2[\sin(\varphi+\psi)\cos\psi - (1+\epsilon)\cos(\varphi+\psi)\sin\psi]. \end{cases}$$

By symmetry, it is sufficient to study the flow around one of the curves of equilibria, say Z_1 (around Z_2 we just have to reverse the arrows). For simplicity, for a fixed ψ_0, we denote the φ component of the equilibria by $\varphi_Z(\psi_0)$, i.e. $\varphi_Z(\psi_0) := \arctan[(1+\epsilon)\tan\psi_0] - \psi_0$. Observe that $(R_{\max}, \varphi_Z(\psi_0), \psi_0)$ are simple roots for $\dot{r}$ and $\dot{\varphi}$. Computing the eigenvalues at $(R_{\max}, \varphi_Z(\psi_0), \psi_0)$, we obtain

$$\begin{cases} \lambda_r = -\dfrac{R_{\max}^3}{R_{\max}^2+2}(-2f'(R_{\max}))[\cos\varphi_Z(\psi_0) + \epsilon\cos(\varphi_Z(\psi_0)+\psi_0)\cos\psi_0] \\ \lambda_\varphi = -2\cos(\varphi_Z(\psi_0)+\psi_0)\cos\psi_0 - \epsilon\sin(\varphi_Z(\psi_0)+\psi_0)\sin\psi_0 \\ \lambda_\psi = 0. \end{cases}$$

Recall that ψ_0 is fixed in $[0, \pi/2]$. If $\psi_0 = \pi/2$, we obtain $\varphi_Z(\psi_0) = \varphi(\pi/2) = 0$ and

$$\begin{cases} \lambda_r = -\dfrac{R_{\max}^3}{R_{\max}^2+2}(-2f'(R_{\max}) > 0 \\ \lambda_\varphi = -\epsilon < 0 \\ \lambda_\psi = 0. \end{cases}$$

Therefore $(R_{\max}, 0, \pi/2)$ is a degenerate saddle. If $\psi_0 \in [0, \pi/2)$, we have

$$\begin{cases} \lambda_r = -(1+\epsilon)\dfrac{R_{\max}^3}{R_{\max}^2+2}(-2f'(R_{\max}))\dfrac{\cos(\varphi_Z(\psi_0)+\psi_0)}{\cos\psi_0} \\ \lambda_\varphi = -(2\cos^2\psi_0 + \epsilon\sin^2\psi_0)\dfrac{\cos(\varphi_Z(\psi_0)+\psi_0)}{\cos\psi_0} \\ \lambda_\psi = 0. \end{cases}$$

Since $\psi_0 \in [0, \pi/2)$ and $\varphi_Z(\psi_0) = \arctan[(1+\epsilon)\tan\psi_0] - \psi_0$, it results that $\varphi_Z(\psi_0) + \psi_0 \in [0, \pi/2)$ and furthermore, $\cos(\varphi_Z(\psi_0)+\psi_0) > 0$. Therefore $\lambda_r > 0$ and $\lambda_\varphi < 0$.

The other cases where $\psi_0 \in (\pi/2, \pi) \cup [\pi, 3\pi/2] \cup (3\pi/2, 2\pi)$ can be treated similarly, reaching the same conclusion, i.e. the equilibria points Z_1 are all degenerate saddles, with

$$\begin{cases} \lambda_r > 0 \\ \lambda_\varphi < 0 \\ \lambda_\psi = 0. \end{cases}$$

□

Lemma 7.4. *The curves of equilibria* C_1 *and* C_2 *on the collision manifold are degenerate saddles (see figure 6). More precisely, for a fixed* ψ_0*, the two corresponding equilibria*

$$(0, \arctan[(1-\epsilon)\tan\psi_0] - \psi_0, \psi_0) \qquad (0, \pi + \arctan[(1-\epsilon)\tan\psi_0] - \psi_0, \psi_0)$$

behave like degenerate saddles.

Proof. The equations of the flow on the collision manifold are

$$\begin{cases} \dot{\varphi} = 2[(1+\epsilon)\sin(\varphi+\psi)\cos\psi - \cos(\varphi+\psi)\sin\psi] \\ \dot{\psi} = 0. \end{cases}$$

As in the previous proof, it is sufficient to investigate the flow around the equilibria curve C_1 (around C_2, by symmetry, we just have to reverse the arrows). Fixing $\psi_0 \in [0, 2\pi)$, we denote the corresponding fixed point on C_1 by $(0, \varphi_C(\psi_0), \psi_0)$ and proceed to calculate its eigenvalues. We obtain

$$\begin{cases} \lambda_r = 0 \\ \lambda_\varphi = 2[(1+\epsilon)\cos(\varphi_C(\psi_0)+\psi_0)\cos\psi_0 + \sin(\varphi_C(\psi_0)+\psi_0)\sin\psi_0] \\ \lambda_\psi = 0. \end{cases}$$

We observe that the vector field (6.1) manifests a degeneracy around $r = 0$. This means that any fixed point on the curve C_1 might have a non-hyperbolic character in the (r, φ) plane. For the moment, let us discuss the sign of λ_φ. Similar to the analysis in the case of the curve Z_1, we fix $\psi_0 \in [0, \pi/2]$. If $\psi_0 = \pi/2$, we have $\varphi_C(\pi/2) = 0$ and therefore $\lambda_\varphi = 2 > 0$. If $\psi_0 \in [0, \pi/2)$, we obtain

$$\lambda_\varphi = \frac{\sin(\psi_0)}{(\varphi_C(\psi_0)+\psi_0)}.$$

Since $(\varphi_C(\psi_0)+\psi_0) = \arctan[(1-\epsilon)\tan\psi_0] \in (0, \pi/2)$, it follows that $\sin(\varphi_C(\psi_0)+\psi_0) > 0$ and therefore $\lambda_\varphi > 0$. The same type of reasoning applies for all the other cases, i.e. for $\psi_0 \in (\pi/2, \pi) \cup [\pi, 3\pi/2] \cup (3\pi/2, 2\pi)$. Therefore we have proved that $\lambda_\varphi > 0$ for any fixed $\psi_0 \in [0, 2\pi)$.

In conclusion, the flow around the equilibria $(0, \varphi_C(\psi_0), \psi_0) \in C_1$ is degenerate, with eigenvalues

$$\begin{cases} \lambda_r = 0 \\ \lambda_\varphi > 0 \\ \lambda_\psi = 0. \end{cases}$$

□

Obviously, the linear approximation of the flow does not provide enough information about the behaviour around the fixed points. Let us take a closer look at the vector field around $(0, \varphi_C(\psi_0), \psi_0) \in C_1$.

Note that on the ψ direction the flow is null, as every point on the circle $\psi \in [0, 2\pi)$ is a parameter for a fixed point. It remains that in order to describe the asymptotical behaviour around $(0, \varphi_C(\psi_0), \psi_0)$, one has to investigate the flow in the (r, φ) coordinates. $\lambda_r = 0$ generates the centre manifold E^c, the span of the zero eigenvector [7, 16]. The general theory ensures the existence of an invariant manifold W^c tangent to E^c at $(r, \varphi_C(\psi_0))$. W^c may not be unique and, usually, it involves a loss of smoothness. Also, around the fixed point, W^c is described by a one-parameter family of curves, i.e. $W^c = \{(r, \varphi) | \varphi = \varphi_\beta(r), \beta \in \mathbb{R}\}$.

In our case, we will compute W^c directly near $(r, \varphi_C(\psi_0))$, as follows (see, for example, [8]): We know that by a proper transformation of coordinates the equations for (r, φ) have the structure

$$\begin{cases} \dot{r} = -\dfrac{r^3}{r^2+2} 2(1 - f(r)) F_1(\varphi, \psi; \epsilon) \\ \dot{\varphi} = \lambda_\varphi(\varphi - \varphi_C(\psi_0)) + \cdots. \end{cases} \tag{7.5}$$

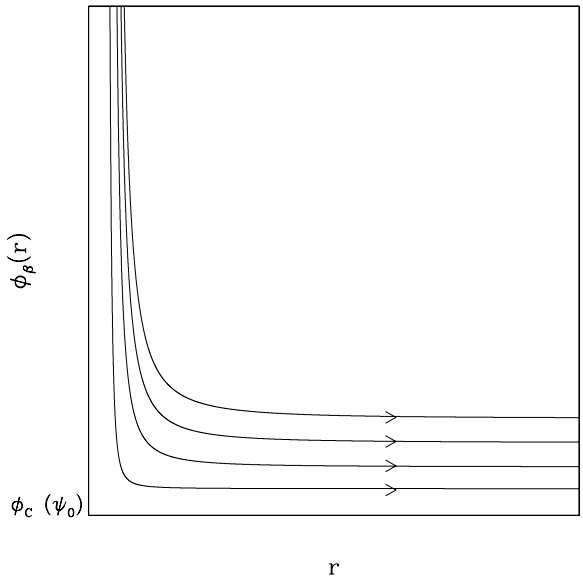

Figure 7. Curves in the $\varphi_\beta(r)$ family around the saddle point $(0, \varphi_C(\psi_0))$.

Near $r = 0$, we can make the approximation

$$\frac{r^3}{r^2+2}2(1-f(r)) = r^3\frac{1}{2}(1+r^2/2+\cdots)2(1-f(r)) = r^3 + \text{higher order terms} \tag{7.6}$$

(note that we are not expanding $f(r)$, a function that is only differentiable, but we are merely looking for the dominant term as r goes to zero). Therefore, around $(r, \varphi_C(\psi_0))$ we have

$$\begin{cases} \dot{r} = -ar^3 + \cdots \\ \dot{\varphi} = \lambda_\varphi(\varphi - \varphi_C(\psi_0)) + \cdots \end{cases} \tag{7.7}$$

where $a := F_1(\varphi_C(\psi_0), \psi_0; \epsilon)$ is a positive number. We obtain immediately that

$$\frac{\mathrm{d}r}{\mathrm{d}\varphi} = -\frac{ar^3}{\lambda_\varphi(\varphi - \varphi_C(\psi_0))} \tag{7.8}$$

with solutions

$$\varphi_\beta(r) = \begin{cases} \beta\, \mathrm{e}^{\lambda_\varphi/(2r^2)} & \text{if} \quad r > 0 \\ 0 & \text{if} \quad r = 0 \end{cases} \tag{7.9}$$

where $\beta \in \mathbb{R}$ is a parameter.

We sketch the family of solutions $\varphi_\beta(r)$ in figure 7. As can be easily seen, the fixed point $(0, \varphi_C(\psi_0))$ is indeed a saddle.

Since the above reasoning applies for any of the points of equilibria, and using lemmas 7.1 and 7.3, we can state the following:

Theorem 7.5. *Let us consider the system (6.1). Then the equilibria are given by the curves C_1, C_2, Z_1 and Z_2, as defined in lemma 7.1, and each of these curves admits a two-dimensional stable manifold and a two-dimensional unstable manifold.*

Corollary 7.6. *In the anisotropic logarithmic problem the Lebesgue measure of the set of initial conditions that lead to collision is zero.*

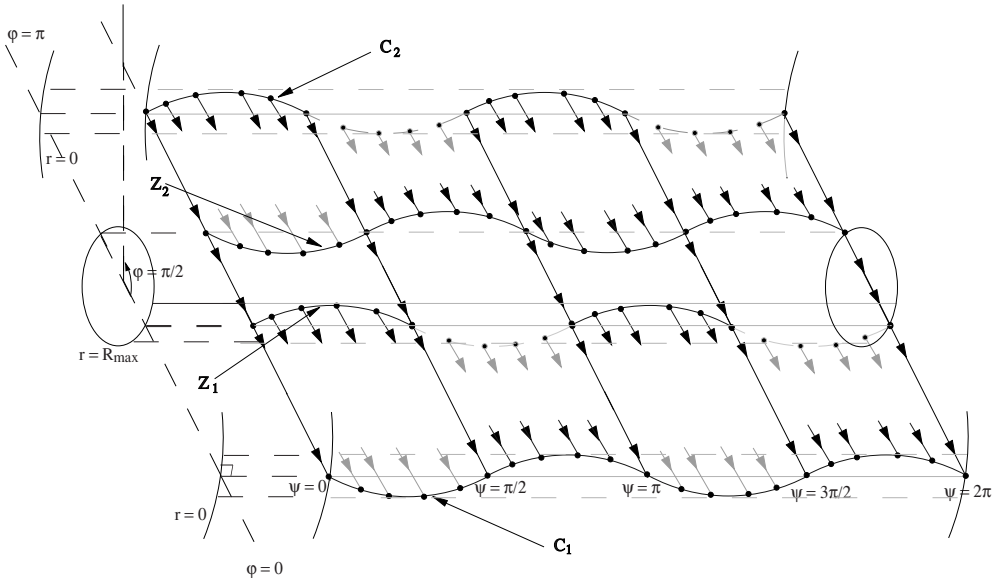

Figure 8. The curves of equilibria C_1, C_2, Z_1, Z_2 under the perturbation ϵ. The arrows show the behaviour of the flow in their neighbourhood. The manifolds C_1 and C_2 intersect transversely along the lines $\sin\varphi = 0$ and $\cos\varphi = 0$.

The last result states that in the phase space the probability of choosing any initial conditions that lead to collision is zero. The set of such initial conditions is formed by a two-dimensional manifold embedded in a three-dimensional phase space. Since we reach a similar conclusion in the isotropic case, we can conclude that for the singular logarithmic potential the anisotropy does not increase the probability of finding orbits falling into the source. In other words, we have proved analytically that in the non-axis-symmetric case all orbits (with the exception of a set with measure zero) are centrophobic, a result that was also noted in previous numerical studies [10].

We now turn our attention to the behaviour of the angular momentum $C(s)$. Recall that $C(s)$ was given in (4.9). For $h = 0$ and in terms of ϵ and (r, φ, ψ), relation (4.9) becomes

$$C(s) = g(r)2[1 - f(r)][(1 + \epsilon)\sin(\varphi + \psi)\cos\psi - \cos(\varphi + \psi)\sin\psi]. \tag{7.10}$$

We note that under the perturbation, the horizontal surface $C = 0$ (see figure 4) splits up, and some of its vestiges are to be found along the two-dimensional stable manifold of C_1 and along the unstable manifold of C_2. In physical space, this corresponds to the case of rectilinear orbits ($C = 0$), which are falling into or ejecting from the source.

The variation of angular momentum (4.14) reads in our coordinates

$$\frac{\mathrm{d}C}{\mathrm{d}s} = -\epsilon g(r)2[1 - f(r)]^{3/2}\sin\psi\cos\psi. \tag{7.11}$$

Since the derivative of C is bounded, there are no 'blow-up' type effects in the evolution of C. Also, since the product $g(r)2[1 - f(r)]$ is always positive, it follows that the critical points of $C(s)$ correspond to $\psi \in \{0, \pi/2, \pi, 3\pi/2\}$ (see figure 8). These orbits, for which $C(s)$ displays a sinusoidal-type behaviour and admits four critical points, represent the family of loop orbits (see also a similar result in the study of Touma and Tremaine [15]).

On the other hand, there are orbits which, under perturbation, will slip in between the stable manifold of C_1 and the unstable manifold of C_2, switching the sign of the angular

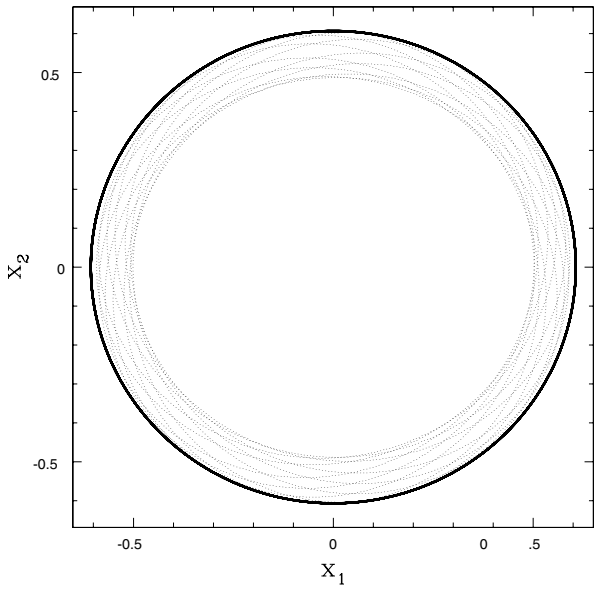

Figure 9. The circle $r = R_0$ (thick line) represents one of the parent families of loop orbits. The dotted line shows the orbital structure that is triggered by applying a perturbation ($\epsilon = 0.1$), to the periodic orbit (shown here is the integration only over a finite time).

momentum. By the nature of the phase space, which is a solid torus, these orbits must wind around indefinitely. These orbits pertain to the family of 'boxlet' orbits discovered by Miralda-Escudé and Schwarzschild [10]. For large perturbations, more and more orbits will break away from the curves of equilibria C_1 and C_2, and become boxlet, a result which was also pointed out in [10]. The separatrix that divides the phase space between loop and boxlet orbits intersects the $(C = 0)$ plane at $\psi = \pi/2$ and $\psi = 3\pi/2$ (see [15]). Some of the orbits that wind up inside the torus will eventually close, becoming the parent orbits of the resonant families (i.e. banana, fish, pretzel, etc) [10].

We do not present here a rigorous proof for the existence of the boxlet obits or the resonances, leaving it for a future study. However, we present below a partial result concerning the orbits which preserve the sign of the angular momentum.

Let us note that the angular momentum can be regarded as a function of two arguments, namely as $C = C(s, \epsilon)$. Then, around the equilibrium point $(s, 0)$, we have the following approximation:

$$C(s, \epsilon) = C(s, 0) + \epsilon \left.\frac{\partial C(s, \epsilon)}{\partial \epsilon}\right|_{\epsilon=0} + O(\epsilon^2) \tag{7.12}$$

or, in our coordinates,

$$C(s, \epsilon) = C(s, 0) + \epsilon g(r) 2[1 - f(r)] \sin(\varphi + \psi) \cos\psi. \tag{7.13}$$

But $C(s, 0)$ is a constant, since this is the case of the unperturbed motion, where the angular momentum is an integral of motion. Denoting $C_0 := C(s, 0)$, it follows that

$$C(s, \epsilon) = C_0 + \epsilon g(r) 2[1 - f(r)] \sin(\varphi + \psi) \cos\psi. \tag{7.14}$$

Since $\epsilon g(r) 2[1 - f(r)] \sin(\varphi + \psi) \cos\psi$ is bounded, we conclude that $C(s)$ preserves its sign for large values of C_0 and small ϵ. This is best noticed near the unperturbed periodic orbits, for example, $(r, \varphi, \psi) = (R_0, \pi/2, \psi)$, $\psi \in [0, 2\pi)$, where $C_0 = \mathrm{e}^{-1/R_0^2} 2\left(1 - R_0^2 \ln R_0\right)$ and where the perturbation induces loop orbits (see figure 9).

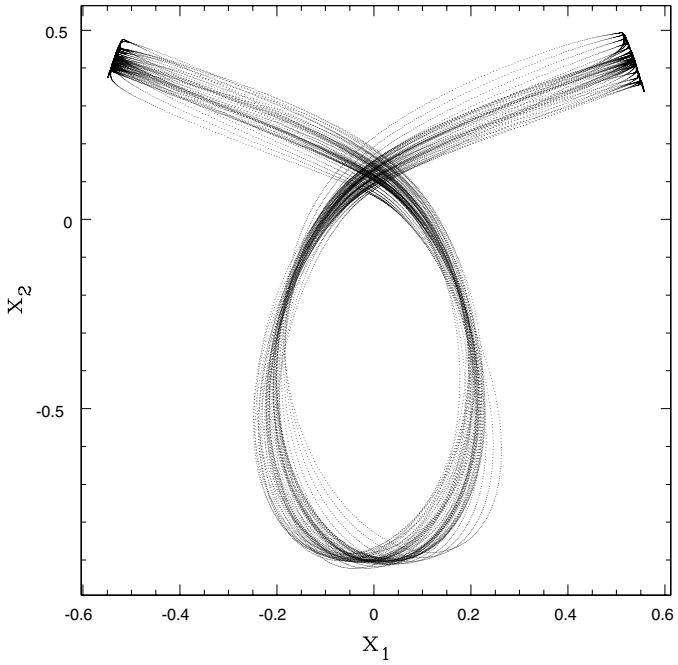

Figure 10. Orbit around the fish (3:2) resonance.

8. The orbital structure

The orbital structure can also be retrieved numerically, by integrating the general form of the system (6.1). The return to the initial coordinates in the physical space, (x_1, x_2), can then be made through the relations

$$\begin{cases} x_1 = q_1/\mu = (1/\mu) r\, \mathrm{e}^{(-1/r^2)} \cos(\varphi + \psi) \\ x_2 = q_2 = r\, \mathrm{e}^{(-1/r^2)} \sin(\varphi + \psi) \end{cases} \tag{8.1}$$

and recalling that the time scale was modified such that both the singularity and the zero-velocity manifold are now reached in an infinite time.

By appropriately choosing the initial conditions and recalling that $\epsilon = \sqrt{\mu} - 1 = 1/b - 1$, one can retrieve the resonance families. For example, we know that the family of loop orbits (1:1) develops around the two periodic orbits $r = R_0$ (see figure 4), i.e. near

$$\begin{cases} x_1 = (1/\mu)\, r\, \mathrm{e}^{(-1/r^2)} \cos(\pi/2 + \psi) \\ x_2 = r\, \mathrm{e}^{(-1/r^2)} \sin(\pi/2 + \psi) \\ \psi = R_0^2 s + \psi_0 \end{cases} \tag{8.2}$$

and

$$\begin{cases} x_1 = (1/\mu)\, r\, \mathrm{e}^{(-1/r^2)} \cos(3\pi/2 + \psi) \\ x_2 = r\, \mathrm{e}^{(-1/r^2)} \sin(3\pi/2 + \psi) \\ \psi = -R_0^2 s + \psi_0. \end{cases} \tag{8.3}$$

The two periodic orbits correspond to the two parent orbits of the loop family, one evolving clockwise ($C < 0$), and the other anticlockwise ($C > 0$). Integrating the system (6.1) for

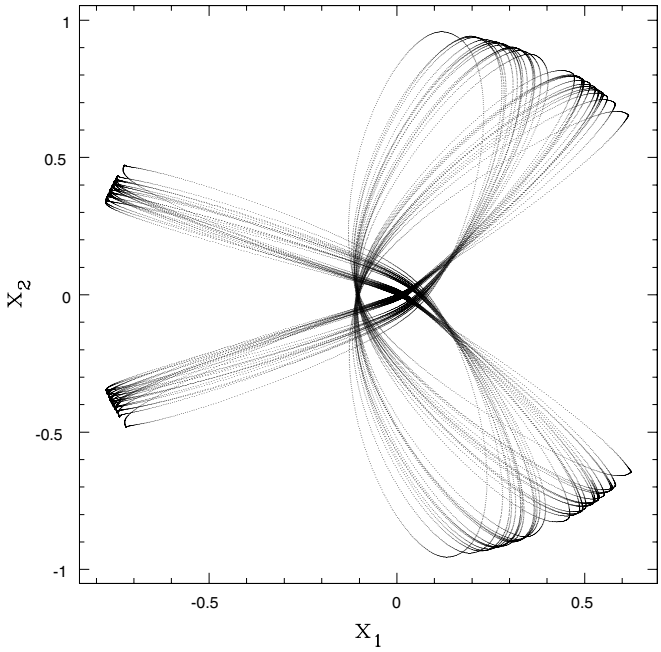

Figure 11. Orbit around the pretzel (4:3) resonance.

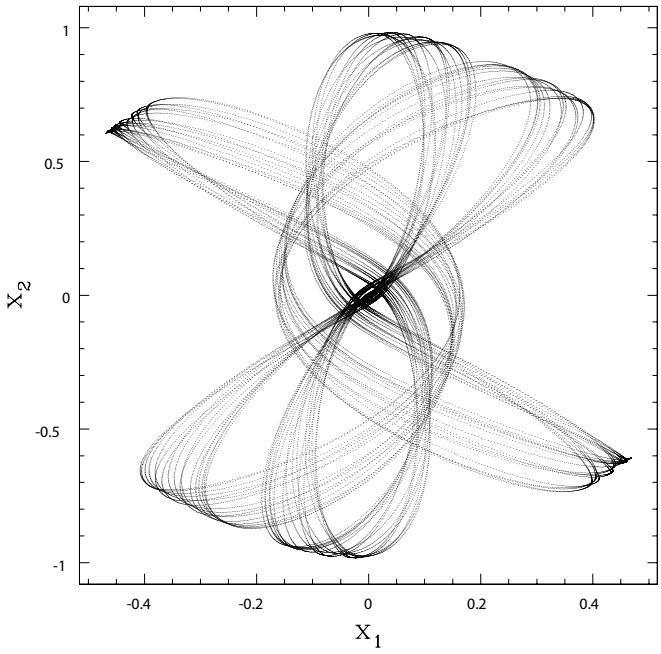

Figure 12. Orbit around the (5:3) resonance.

the case $\epsilon = 0$, around either $(R_0, \pi/2, \psi)$ or $(R_0, 3\pi/2, \psi)$, one retrieves a circle of radius R_0, as indicated with thick line in figure 9. The same figure shows, with dotted line, the

orbital structure in the vicinity of the parent orbit for the case when $\epsilon = 0.1$ (corresponding to $b = 0.9$).

Besides the loop resonance, several other resonances can be recovered from the new system of differential equations. We remark that under large perturbations (i.e., large deviations from axis-symmetry), the families of minor orbits will occupy more and more of the phase space. We do not attempt here to cover the entire phase space, but rather give a few examples of families of minor orbits found with our new system of equations. For example, figure 10 shows an example of an orbit around the fish (3:2) resonance, in the case $\epsilon = 0.3$ (corresponding to $b = 0.7$) and the initial conditions $r = 0.9$, $\varphi = \pi/12$ and $\psi = \pi/8$. Figure 11 shows an orbit around the pretzel (4:3) resonance, when $\epsilon = 0.1$ and $r = 0.45$, $\varphi = 0$, $\psi = \pi/14$. Figure 12 shows an orbit near the (5:3) resonance, obtained for $\epsilon = 0.3$, $r = 0.4$, $\varphi = \pi/12$, $\psi = \pi/6$. We note however, that these parameters should be taken only as a guidance for the location of the resonances.

9. Conclusions

Previous numerical studies have revealed several important aspects of the orbital structure of the logarithmic potential: the division between loop and box orbits, the presence of resonances, the scattering effect of the singularity (which renders the box orbits unstable) and the transition to chaos. We have performed an analytical study of the singular logarithmic potential and proved several of these results.

We summarize our results as follows:

- We provide a description of the dynamics near the singularity and at the maximum distance from the source permitted for a given level of energy.
- In the axis-symmetric case, we retrieve the complete global dynamics of the orbits and describe it on a solid torus bounded by the two surfaces $\{r = 0\}$ and $\{r = R_{\max}\}$. We find analytically the two periodic orbits $r = R_0$, which correspond in physical space to the two parent families of the loop orbits (in clockwise and respectively, in anticlockwise motion).
- In the non-axis-symmetric case, we prove that all orbits, except a negligible set, are centrophobic—a result that has been originally discovered in the numerical study of Miralda-Escudé and Schwarzschild [10].
- In the same non-axis-symmetric case, we show that there exist orbits which preserve the sign of the angular momentum and retrieve the loop resonance. Finally, we also show how several other minor family orbits can be obtained from our new system of equations.

The analytical description in general non-axis-symmetric case remains still open, several problems requiring further investigation. One of them is the retrieval of the family of boxlet orbits, which are known to dominate the dynamics near the singularity [10]. We conclude, however, that under large perturbations (large deviations from axis-symmetry), most of the phase space is occupied by orbits that slip in between the stable manifold of C_1 and the unstable manifold of C_2 and wind around indefinitely. Most of these orbits pertain to the family of the boxlet orbits. Some of these winding orbits may be closed and would lie at the origin of the resonant families observed experimentally. Further work in this direction will have to include an in-depth analysis of resonances in the (x_1, x_2) variables and a Fourier expansion of the periodic solutions for $r(s)$.

Another aspect that remains to be clarified is the existence of the stochastic orbits near the singularity and the transition to chaos. The analytical study in this case is hindered by the fact that the system given by the Hamiltonian (2.1) does not admit any hyperbolic equilibrium

points, and therefore, the perturbative methods which are usually employed in proving the existence of chaos (including the Melnikov method [9]) become unapplicable. We note that the Melnikov method has been used in the past in the case of the logarithmic potential [5], however not on the exact Hamiltonian, but on the integrable Stäckel Hamiltonian [12]. Understanding the onset of chaos in the singular logarithmic potential is a very important problem for the construction of galaxy models based on libraries of orbits (see, for example, [14]), in which generally, it is *a priori* assumed that the stochastic orbits play a negligible role.

References

[1] Binney J and Spergel D 1982 *Astrophys. J.* **252** 308
[2] Binney J and Tremaine S 1987 *Galactic Dynamics* (Princeton, NJ: Princeton University Press)
[3] Karanis G I and Caranicolas N D 2001 *Astron. Astrophys.* **367** 443
[4] Devaney R L 1978 *Inventiones Math.* **45** 221–51
[5] Gerhard O E 1986 *Mon. Not. R. Astron. Soc.* **222** 287
[6] Gerhard O E and Binney J 1985 *Mon. Not. R. Astron. Soc.* **216** 467
[7] Guckenheimer J and Holmes P 1985 *Nonlinear Oscillations, Dynamical Systems and Bifurcations of Vector Fields* (New York: Springer)
[8] Kuznetsov Y A 1995 *Elements of Applied Bifurcations Theory* (New York: Springer)
[9] McGehee R 1981 *Comment. Math. Helv.* **56** 524–57
[10] Miralda-Escudé J and Schwarzschild M 1989 *Astrophys. J.* **339** 752
[11] Richstone D 1982 *Astrophys. J.* **252** 496
[12] Stäckel P 1890 *Math. Ann.* **35** 91
[13] Stoica C 2002 *Celest. Mech. Dyn. Astr.* **84** 223
[14] Schwarzschild M 1979 *Astrophys. J.* **232** 236
[15] Touma J and Tremaine S 1997 *Mon. Not. R. Astron. Soc.* **292** 905
[16] Wiggins S 1990 *Introduction to Applied Nonlinear Dynamical Systems and Chaos* (New York: Springer)